nature geoscience

SUPPLEMENTARY INFORMATION

DOI: 10.1038/NGEO2681

Anthropogenic carbon release rate unprecedented during the past 66 million years

Richard E. Zeebe[1,*], Andy Ridgwell[2,3], and James C. Zachos[4]

*Corresponding Author.

[1]School of Ocean and Earth Science and Technology, University of Hawaii at Manoa, 1000 Pope Road, MSB 629, Honolulu, HI 96822, USA. zeebe@soest.hawaii.edu

[2]School of Geographical Sciences, University of Bristol, UK. andy@seao2.org

[3]Department of Earth Sciences, University of California, Riverside, USA.

[4]Earth and Planetary Sciences Department, University of California, Santa Cruz, USA. jzachos@ucsc.edu

S1 Time-series analysis (stationary)

For the stationary (transformed) time series we determine possible systematic leads/lags across the full Millville carbon and oxygen isotope records using time-series analysis. The raw data series ($X = \delta^{13}$C, $Y = \delta^{18}$O) are non-stationary and inadequate for determining leads/lags based on autocorrelation function (ACF) and cross-correlation function (CCF)[1,2]. Thus, we use first-order differencing:

$$x_i = X_{i+1} - X_i \; ; \qquad y_i = Y_{i+1} - Y_i \; . \tag{1}$$

The normalized CCF sequence of length $2N-1$ is given by:

$$r_{xy}(k) \;=\; c^{-1} \sum_{i=1}^{N-k} \tilde{x}_i \cdot \tilde{y}_{i+k}/N \; ; \qquad k = 0, 1, \ldots, N-1 \tag{2}$$

$$r_{xy}(k) \;=\; c^{-1} \sum_{i=1-k}^{N} \tilde{x}_i \cdot \tilde{y}_{i+k}/N \; ; \qquad k = -1, -2, \ldots, -(N-1) \tag{3}$$

where

$$c = \sqrt{\sum \tilde{x}_i^2/N \cdot \sum \tilde{y}_i^2/N} \tag{4}$$

and $\tilde{x}_i = x_i - \overline{x}$, $\tilde{y}_i = y_i - \overline{y}$ are deviations from the respective means. Significant r_{xy} at $k > 0$ indicate leads of x over y.

The ACFs of the differenced series (see main manuscript) are similar to white-noise ACFs, except for significant negative correlations (95% level) at $\Delta k = \pm 1, \pm 2$, which can lead to biases in the CCF[1–3]. Thus, the x and y series were prewhitened, using an autoregressive (AR) process of order $p = 6$, AR(6), which yields the x' and y' series (see main manuscript). We choose $p = 6$, as $p \geq 6$ is necessary to obtain white-noise ACFs for x' and y'.

Briefly, prewhitening of time series removes spurious correlations introduced into the CCF due to significant autocorrelations in the individual time series (for

details, see refs. 1–3). For example, consider the process X_t with mean $\mu = 0$ given by:

$$X_t = \alpha\, X_{t-1} + Z_t\,, \tag{5}$$

where α is a constant and Z_t is a purely random process with mean zero. X_t is called an autoregressive process of order one, AR(1). Given N observations (time series x_t), the parameters μ and α can be estimated by, say, least squares. Assume for simplicity $\overline{x}_t = \mu = 0$, then the prewhitened (or filtered) time series is given by[2,3]:

$$x'_t = x_t - \alpha\, x_{t-1}\,. \tag{6}$$

Thus, the filtered time series consists of the residuals of the fit model. If the underlying process is indeed an AR(1) process, then x'_t will be white noise and for large N its ACF coefficients $r_k \simeq 0$ ($k \neq 0$), with mean $\simeq$ zero and variance 1/N. In summary, prewhitening effectively removes autocorrelation from a time series and may need to be applied before calculating cross-correlations between time series.

S2 Apparent leads and lags

Visually, the graphs representing the %response of the raw, non-stationary isotope records at Millville may suggest apparent δ^{18}O leads over δ^{13}C during some intervals and apparent lags during others (Fig. 3). However, as the time series analysis shows, no significant leads/lags are detected, except for a contemporaneous correlation ($\Delta k = 0$, see main manuscript). Apparent visual leads/lags between two non-stationary time series can be easily generated if, for instance, their relative trends differ across some interval; yet their relationship may be perfectly contemporaneous (see Fig. S1a, for example). In fact, in the example shown, the detrended series are identical. At Millville, the differenced (or detrended) δ^{18}O and δ^{13}C series are

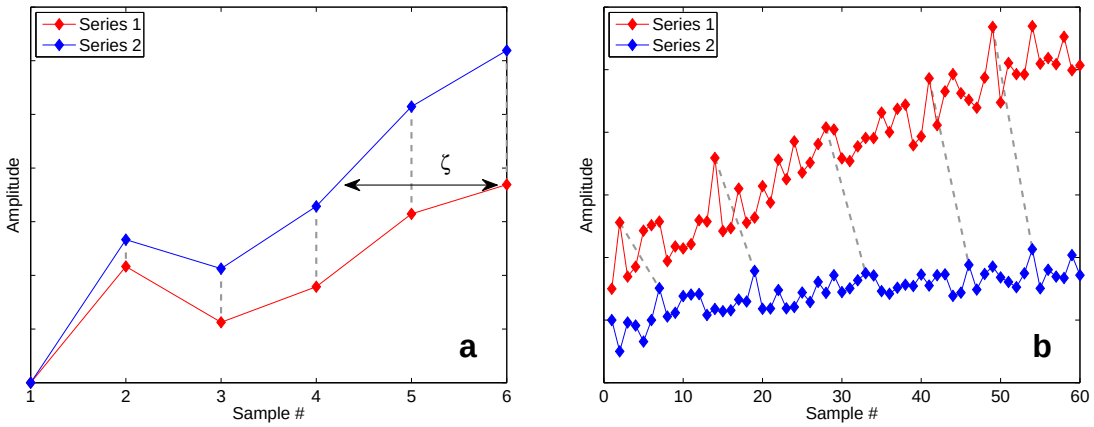

Figure S1. Time series examples. (a) Contemporaneous relationship ($\Delta k = 0$, dashed lines), visually suggesting Series 2 to lead over 1 (label ζ) due to different relative trends. The apparent lead disappears after detrending (detrended series are identical). (b) Series 1 leads over 2 by $\Delta k = 5$ (dashed lines).

not identical. However, the situation is similar. Systematic changes and noise from global/local climate/carbon cycle processes, proxy recording, etc. affect the individual series differently. Hence, it is not to be expected that the series will show the *same relative amplitude of change* across all intervals. It is the timing and the sign of the changes in the two series (e.g., alignment of characteristic features, see Figs. 2 and S1b) that is critical to determine lead-lag relationships in noisy time series, rather than the relative amplitude of the changes.

For the model output (Fig. 3), lead-lag determination using cross-correlation is unsuitable because of the mostly smooth curves and large individual autocorrelation, which leads to bias in the cross-correlation[1–3]. In fact, model lead-lag determination is less complex (Section S8) because the models were forced by a simple, known function. Also, the models do not exhibit internal noise from climate/carbon cycle dynamics, neither is noise from 'proxy recording' involved at the output grid-points/boxes. Thus, the model lead-lag relationship can be directly determined from the normalized response (Fig. 3, Section S8).

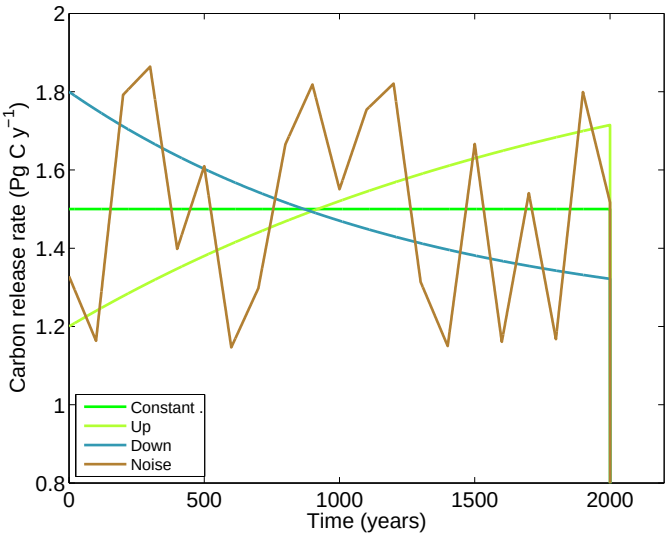

Figure S2. Different carbon release patterns at input time $t_{\mathrm{in}} = 2,000$ y and the same total carbon input of 3,000 Pg C yr^{-1} for all scenarios. The 'Noise' scenario is based on a constant mean value and random noise added on a 100-year time scale.

S3 Sedimentation rate and carbon release pattern

Our approach yields a time constraint for the minimum *overall* onset interval and is thus based on an *average* sedimentation rate $\bar{r}_{\mathrm{sed}}$ (see main manuscript). Importantly, however, we do not require the sedimentation rate, $r_{\mathrm{sed}}(t)$, to be constant over time. First, our time-series analysis is based on the cross-correlation function (CCF), which does not explicitly depend on space or time coordinates (z_i, t_i) at which the measurements were taken (Eqs. 2, 3). This CCF property is intuitively obvious because the time series variables ($X = \delta^{13}\mathrm{C}$, $Y = \delta^{18}\mathrm{O}$) are both measured at the same z_i for all i, making the actual z_i values irrelevant for the correlation. Thus, even if the sedimentation rate varied widely, it has no effect on the cross-correlation function and hence no effect on the lead/lag relationship we have obtained in the depth-domain (Δk).

Second, it is important that the Δk were derived from the analysis of the *entire* time series and hence represent an overall correlation across the onset. The Δk are

not to be confused with individual leads/lags that may change from one part of the series to another. If those were translated into the time domain, then variations in $r_{\mathrm{sed}}(t)$ would indeed matter. But this is not the case. Our method first determines the overall lead/lag in the depth-domain and translates it into an overall lead/lag in the time-domain, considering (and ultimately determining) the total time represented across the onset. Our method is not primarily designed to determine whether parts of the onset were completed slower or faster than average due to variations in $r_{\mathrm{sed}}(t)$. However, if the pacing did vary, say, systematically across the onset, then we would find significant correlations at different Δk, for example, during the first and second half of the onset. This is also not the case. During the first half, we do not find a significant correlation at any Δk (not shown), consistent with the inconclusive lead/lag correlation of the raw (non-stationary) time series across the start of the onset, as discussed in the main manuscript. During the second half, we find a significant correlation at $\Delta k = 0$, i.e. the same as for the entire onset and the complete time series (see main manuscript). In summary, the sedimentation rate is (i) unlikely to have varied systematically across the onset and (ii) if varied, has no effect on our *overall* lead/lag relationship.

One factor that can indirectly cause variations in sedimentation rate and, more directly, in the timing of the recorded δ^{13}C and δ^{18}O is the pattern of the carbon release over time. Given a total integrated carbon release, the simplest assumption is a constant release rate R_{C}, which we have used in our standard model scenarios. However, this assumption can easily be relaxed and the effect on the calculated model time lag (τ_{mod}) be tested. Hence in addition to a constant carbon release rate, we tested (1) an increasing rate, (2) a decreasing rate, and (3) a rate with constant mean plus random noise (Fig. S2). For each given total carbon input and model

release time, t_{in}, the three scenarios were adjusted to yield the same total carbon input. Certainly, more extreme scenarios could be imagined such as a linear increase starting at $R_C = 0$ Pg C yr^{-1} or a Gauss peak centered halfway across the onset. However, such scenarios would substantially alter the effective t_{in}, which should then be reduced to, say, half the onset interval or the width of the Gauss curve. These scenarios are thus covered under shorter average release time, rather than release pattern. The tests were performed with LOSCAR and indicate a sensitivity to the release pattern similar to the sensitivity to other parameters (see Fig. 4 and Section S9 for discussion).

S4 Bulk carbonate diagenesis

We assume the bulk carbon isotope records from the New Jersey siliciclastic sequences capture the relative timing of the CIE with respect to climate (i.e., $\delta^{18}O$). This assumption is supported by the observation that, for instance, the Millville bulk isotope records are consistent with data from planktonic foraminifera at the same site[4]. However, we recognize that absolute values are not necessarily representative of the values of seawater DIC. This recognition is based on previous studies of NJ margin cores which show that bulk carbonate $\delta^{13}C$ can be offset toward lower values relative to planktonic foraminifera from the same samples, say at Wilson Lake[5,6] (Fig. S3). This offset is not constant over time or in space, increasing within the CIE and with proximity of the core to the coastline, suggesting that a process associated with either reworking or diagenesis is responsible. In samples within the CIE the bulk $\delta^{13}C$ is often several per mil lower than values for planktonic foraminifera. The low $\delta^{13}C$ bulk values recorded in several cores reflect either the presence of authigenic and/or diagenetic carbonate phases.

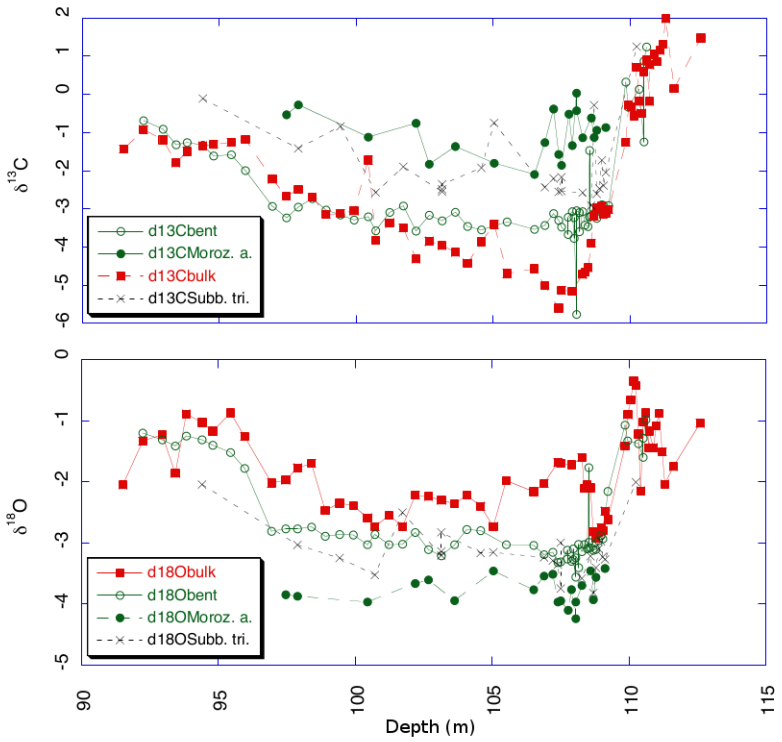

Figure S3. Bulk and foraminifer isotope data at Wilson Lake across PETM onset, main-, and recovery phase.[5,6]. bent = benthic, Moroz. a = *Morozovella aequa*, **Subb. tri. =** *Subbotina triangularis*.

The upper Paleocene and lower Eocene facies of the NJ Margin sequences are comprised predominantly of clays and silts with very minor amounts of carbonate due to the high input of siliciclastics, particularly within the CIE interval (Marlboro Clay). The low porosity clays retard carbonate recrystallization related to diagenesis, particularly meteoric, and as a consequence, the preservation of foraminifer shells is generally excellent. The high sedimentation rates, however, likely promoted bacterial mediated sulfate reduction and the formation of authigenic carbonate phases such as siderite[7,8]. Because the carbon is sourced from respired organic matter, the $\delta^{13}C$ is much lower than that of biogenic carbonate phases[9,10]. The increased flux of siliciclastics tends to promote authigenic carbonate formation while diluting

biogenic carbonate, thus shifting the bulk $\delta^{13}C$ toward lower values. This scenario is supported by the relatively high $\delta^{18}O$ values consistent with early diagenesis in the presence of seawater (for instance, at Wilson Lake, Fig. S3). In contrast, bulk $\delta^{13}C$ and $\delta^{18}O$ at Millville[4] and at Bass River more closely track foraminiferal values[6,11,12] (see Fig. 1). The extent to which the Millville bulk isotope records might be affected by early diagenesis is not precisely known. However, we note that both absolute isotope values and excursions ($\sim$3‰ in $\delta^{13}C$ and $\sim$1‰ in $\delta^{18}O$, indicating $\sim$5 K warming) are consistent with most other pelagic sequences[13] and foraminiferal data from Bass River[6,11,12] (Fig. 1). Most importantly, the Millville bulk isotope records are consistent with data from planktonic foraminifera at the same site[4], which lends confidence in our approach as foraminifera are considered robust recorders of changes in $\delta^{13}C$ and $\delta^{18}O$. Moreover, diagenetic processes would alter the magnitude of the signals, rather than the relative timing of change.

Finally, we emphasize that the resolution of other PETM sections across the onset (including at Bass River and Wilson Lake) is currently insufficient to determine leads and lags between $\delta^{13}C$ and $\delta^{18}O$. We hence use the Millville record as the target for our approach and derive an estimate for the maximum sustained rate of carbon release across the PETM onset.

S5 Couplets, contamination, cycles, and bioturbation

Wright and Schaller[14] described rythmic 'couplets' in the Millville core, subsequently identified as artifacts of drilling disturbance, so-called biscuiting or core discing[15]. As a result of core discing, drilling slurry can be injected between the discs, potentially leading to sample contamination from the slurry with a distinct $\delta^{18}O$ signature (we discuss $\delta^{18}O$ in the following but found essentially the same results

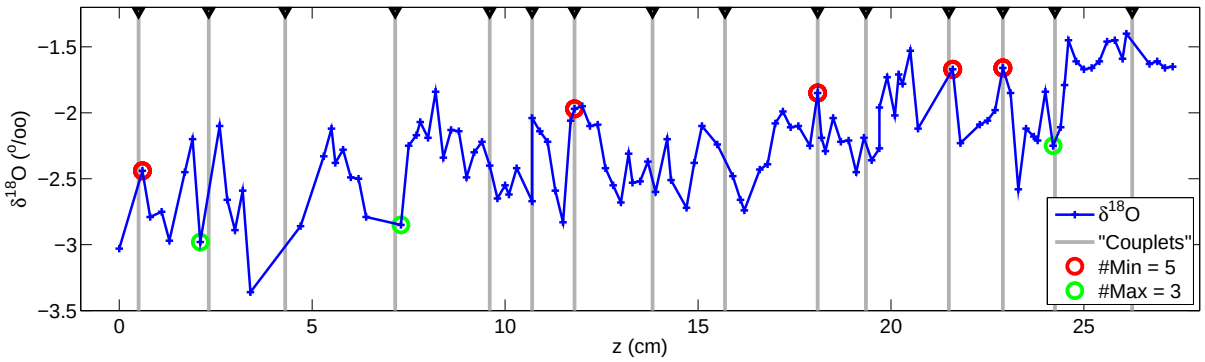

Figure S4. δ^{18}**O and couplet positions (black triangels, gray lines) across the PETM onset at Millville[14]. The dominant couplet spacing or period is** $P \simeq 2$ **cm. Note reversed y-scale (minima point upwards).**

for δ^{13}C). If so, one would expect either anomalously light or heavy δ^{18}O values associated with the couplets. This is not the case (Fig. S4). Visual inspection reveals that five minima and three maxima occur close to 8 out of 15 couplets across the onset (note reversed y-scale). The relationship between the remaining 7 couplets and δ^{18}O extrema is inconclusive. Hence there is no systematic relationship between couplets and light/heavy δ^{18}O values, providing no obvious evidence for contamination.

We also tested if a potential contamination could have affected δ^{18}O values more subtly by imprinting a cyclicity on δ^{18}O associated with the dominant couplet frequency of ∼0.5 cycles/cm (14 cycles/27 cm, mean period $P \simeq 2$ cm). Given that the couplets resulted from core discing, a spectral peak at the couplet frequency is not to be expected, except if contamination occurred or if the primary δ^{18}O record coincidentally carried a signal at the same frequency. However, spectral analysis using the multi-taper method and background noise estimation[16] shows *reduced* power at the mean couplet period $P \simeq 2$ cm (Fig. S5). In fact, the noise background estimate shows that the spectrum is consistent with simple red noise (same for δ^{13}C). The peak at $P \simeq 3$ cm is barely significant at the 99% confidence level (CL) and is not surprising as $M \times 0.01 \simeq 0.6$ random peaks >99% CL are to be expected, where

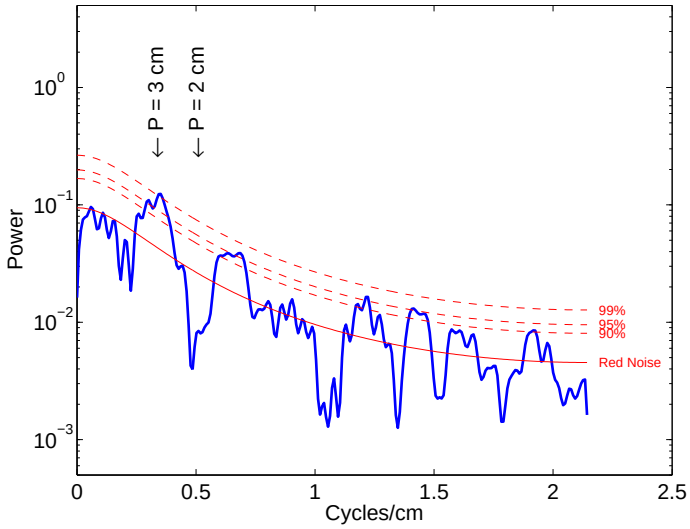

Figure S5. Multi-taper spectrum of δ^{18}O across the PETM onset at Millville. The dominant couplet period is $P \simeq 2$ cm.

$M = 59$ is the number of independent frequencies extracted from the $N = 118$ data points across the onset. Also, the peak at $P \simeq 3$ cm can not be associated with a potential split of the couplet frequency into two bands. All distances between individual couplets are <2.85 cm.

Thus, we also do not find evidence for cycles associated with the couplets from potential contamination or other factors. In fact, we do not find evidence for any dominant cycles at all in both δ^{18}O and δ^{13}C. Any strong harmonic signal in the record (such as the annual cycle) would produce a large spectral peak $\gg$99% CL. Wright and Schaller[14] indeed suggested the imprint of the seasonal cycle on δ^{18}O. However, a spectral analysis was not presented, rather the output from a filter with too narrow a bandwidth ($\pm$2%).

Finally, the features of the isotope record (Fig. S4) also address concerns about potential effects of bioturbation and sediment mixing across the onset record at Millville. The δ^{18}O record shows significant fluctuations (consistent with red noise) of up to $\sim$1‰, which are resolved by *multiple* data points across mm to cm scale (Fig. S4).

For example, at $z = 12 - 13$ cm and $15 - 16$ cm, the increases in $\delta^{18}O$ are resolved by 5 and 4 data points, respectively (note reversed y-scale). Bioturbation/mixing would smooth, homogenize, or eliminate such features across cm scale. Thus, if bioturbation and/or sediment mixing did occur across the onset, the effect on the isotope records is likely small.

S6 GENIE model

We used the Earth system model cGENIE[17] in its late Paleocene configuration as described in ref. 18. The only changes we make are firstly to enable temperature-dependent silicate and carbonate weathering and apply a background rate of volcanic CO_2 emissions, all as described in ref. 19. In this setup, terrestrial carbonate and silicate weathering are split 1:1 in order to balance a total global $CaCO_3$ burial flux of 14.7 Tmol Ca^{2+} yr^{-1} (i.e. 7.35 Tmol Ca^{2+} yr^{-1} each), with a CO_2 volcanic outgassing rate of 7.35 Tmol Ca^{2+} yr^{-1} to balance silicate weathering. The second change we make compared to ref. 18 is to create a shallow shelf region corresponding to the paleo vicinity of Millville, comprising a single new ocean grid point with 81 m water depth (the uppermost layer in the cGENIE ocean circulation model). Also, we add two new ocean grid points at 175 m water depth (the uppermost two ocean model layers) adjacent to the grid point representing Millville's paleo-location (cf. star in Fig. S6). As per ref. 17, we first spin-up the climate system and atmosphere-ocean-sediment carbon cycle for 20 kyr as a 'closed system', with weathering set to automatically track carbonate burial and with atmospheric CO_2 prescribed to be 836 ppmv and $\delta^{13}C = -4.9‰$ (ref. 18). This is followed by 100 kyr of 'open system' spin-up with terrestrial weathering now allowed to freely respond to climate. In this open system phase, $\delta^{13}C$ of volcanic CO_2 is set at $-6‰$ and weathered carbonates are

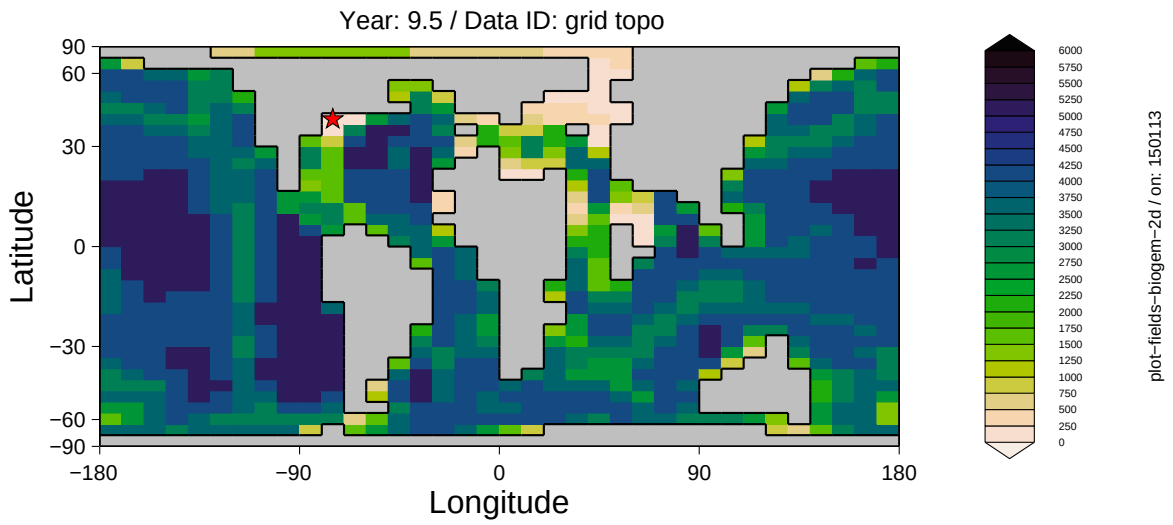

Figure S6. Bathymetry used in our PETM simulations with GENIE to determine model time lags (see main manuscript). We analyzed GENIE's global mean properties as well as GENIE's grid-point output on the North-West Atlantic shelf (NWA-shelf, corresponding to Millville's paleo-location, red star).

simply assigned an isotopic value in order to balance the global isotopic budget in the absence of marine organic carbon burial (necessitating a δ^{13}C value of 13.58‰). All subsequent experiments (including a control) are run for a duration of 10 kyr, following on from the end of the 100 kyr, 2nd-stage spin-up. In addition to global mean sea-surface temperature (SST) and δ^{13}C, we analyzed GENIE's grid-point output on the North-West Atlantic shelf (NWA-shelf, corresponding to Millville's paleo-location, Fig. S6).

S7 LOSCAR model

The LOSCAR model (Long-term Ocean-atmosphere-Sediment CArbon cycle Reservoir model) computes the partitioning of carbon between ocean, atmosphere, and sediments on time scales ranging from centuries to millions of years[20,21].

LOSCAR couples ocean-atmosphere routines to a computationally efficient sediment module. This allows adequate computation of $CaCO_3$ dissolution, calcite compensation, and long-term carbon cycle fluxes, including weathering of carbonate and silicate rocks. The ocean component includes biogeochemical tracers such as total carbon, alkalinity, phosphate, oxygen, and stable carbon isotopes. LOSCAR's configuration of ocean geometry is flexible and allows for easy switching between modern and paleo-versions. The global ocean is geometrically divided in LOSCAR into separate ocean basins representing Atlantic, Indian, and Pacific Ocean (plus Tethys in the Paleocene/Eocene-version). In turn, each ocean basin is subdivided into surface, intermediate, and deep ocean. In addition, the model includes a generic high-latitude box, representing cold surface waters. The Paleocene/Eocene ocean bathymetry in LOSCAR is based on ref. 22. The model's architecture, its components, tuning, and examples of input and output are described in detail in ref. 21. Additional parameterizations necessary to calculate model time lags such as a climate response function for different values of climate sensitivity are described in ref. 23.

S8 Percent response at which to determine model time lag

As mentioned in the main manuscript, simulated $\delta^{13}C$ leads the model climate response at the onset's start because the models are forced by carbon input. In reality, temperature may have led carbon input initially[24,25], although the data do not support any significant $\delta^{18}O$-lead at the start (Fig. 2d). Nevertheless, to avoid potential model bias during the initial onset phase, we omit the first 40% of the normalized $\delta^{13}C$ (X) and temperature (Y) rise when determining the model time lag. Furthermore, note that the end of the onset interval in the data record could be located within the data gap (Fig. 2). Hence, we also omit the final 20% when determining

τ_{mod}. As a result, we calculate τ_{mod} as the average model time lag between 40% and 80% response of X and Y. The averaging produced smoother τ_{mod} sequences for different carbon release times, as the increase in both X and Y with time is generally non-linear (Fig. 3).

In cases when the model output was stored at discrete times t_i and coarse Δt_i, then X_i and Y_i were first interpolated onto a fine time axis (e.g., at 1-yr resolution, index j). Next, the times were determined at which X_j and Y_j were closest to percent-values (index p) between 40% and 80% (e.g., in steps of 1%), yielding the model time lags at a given percentage:

$$\tau_{\mathrm{mod}}^{p} = t_{Y}^{p} - t_{X}^{p} \,, \tag{7}$$

where $p = 1, \ldots, K$ (and e.g., $K = 41$). Finally, the average model time lag between 40% and 80% response in normalized δ^{13}C and temperature is given by:

$$\tau_{\mathrm{mod}} = \frac{1}{K} \sum_{p=1}^{K} \tau_{\mathrm{mod}}^{p} \,. \tag{8}$$

S9 Sensitivity of minimum onset interval to parameter variation

To evaluate the sensitivity of the calculated minimum onset interval to parameter variations, we focus on the calculated model lag, τ_{mod}. We consider effects of various parameters and assumptions, including model release time, release pattern, total carbon input, climate sensitivity, initial $p\mathrm{CO}_2$, and atmospheric vs. deep-ocean carbon injection (for the last item, see Section S10). The model release time was varied in both models, GENIE and LOSCAR. However, full runs for all parameter variations are time-consuming with GENIE and were hence performed with LOSCAR (computationally much less expensive)[21,23]. LOSCAR uses a climate response function parameterization[23], which may produce less accurate results than

GENIE when the forcing is changing with time. The runs showed that LOSCAR's τ_{mod} are similar, albeit mostly larger, than GENIE's τ_{mod} (see main manuscript). Nevertheless, the LOSCAR results provide insight into the general effect of various parameters on the calculated minimum onset interval. Note that because all LOSCAR runs yielded τ_{mod} larger than the GENIE scenario on the North-West Atlantic shelf (main manuscript), our estimate of 4,000 yr for the minimum onset interval remains unchanged.

At very short release times, τ_{mod} approaches a finite value, corresponding to instant release (see Fig. 4). The model lag then increases with release time on century time-scale until reaching a maximum on millennial time-scale. Subsequently, the release becomes slow enough for the climate response to keep up with the forcing and the model lag drops. Eventually, τ_{mod} intercepts τ_{dat} (the lag allowed by the data records), yielding the minimum carbon release time (arrow, Fig. 4).

Standard model runs with both GENIE and LOSCAR use 3000 Pg C carbon input and climate sensitivity $S_{2\times} = 3$ K per CO_2 doubling; the initial atmospheric CO_2 concentration in the standard runs with GENIE and LOSCAR is 836 and 1000 ppmv, respectively. The total carbon input has a small effect on the calculated τ_{mod} in LOSCAR (Fig. 4) as the carbon-cycle-, climate forcing-, and climate response all somehow scale with the amount of carbon released. The different carbon release patterns (Fig. S2) have a moderate effect on the calculated τ_{mod} (Fig. 4). The increasing (decreasing) rates give somewhat shorter (longer) τ_{mod}. The reason is that, for example, a higher rate at the start of the onset (declining subsequently) causes a more rapid initial ^{13}C excursion and hence a larger lead relative to the climate response, similar to a shorter release time. As might be expected, the random noise scenario produces variations, but no consistent trend in τ_{mod} relative to the standard

scenario.

Higher climate sensitivity causes the model lag to rise, which is expected from basic feedback analysis[26,27]. If anything, climate sensitivity during the PETM was higher than 3 K, not lower[20,23], again suggesting that our minimum onset interval holds, even if $S_{2\times}$ was higher than 3 K. Lowering the initial $p\mathrm{CO_2}$ from 1,000 to 750 ppmv in LOSCAR lowers τ_{mod} to values closer to GENIE's τ_{mod}, which is initiated at 836 ppmv. At lower initial $p\mathrm{CO_2}$ both the normalized model $\delta^{13}\mathrm{C}$ and $p\mathrm{CO_2}$ response are more rapid because of lower initial DIC, which makes the system more sensitive to the perturbation (at the same carbon input). However, due to non-linearities in carbonate chemistry, the speedup in the $p\mathrm{CO_2}$ response slightly outpaces that in $\delta^{13}\mathrm{C}$. Hence τ_{mod} drops slightly. Overall, the effect is small and given the pre-PETM Eocene warmth, an initial $p\mathrm{CO_2}$ of 750 ppmv is probably a lower limit, meaning that also varying this parameter does not alter our 4,000 yr-estimate for the minimum onset.

S10 Long release time: Model temperature leads $\delta^{13}\mathrm{C}$

As mentioned in the main manuscript, for long release times τ_{mod} reverses sign, i.e. the model temperature starts leading $\delta^{13}\mathrm{C}$, which may appear counterintuitive. The reason is as follows. For release times shorter than a few millennia, surface-ocean $\delta^{13}\mathrm{C_{DIC}}$ initially drops rapidly in response to the release of isotopically light carbon (the normalized %response rises, Fig. S7a). Note that:

$$\delta^{13}\mathrm{C_{DIC}} = \left(\frac{\mathrm{DI^{13}C/DIC}}{R_{std}} - 1 \right) \times 1,000 \,. \tag{9}$$

Hence for $\delta^{13}\mathrm{C_{DIC}}$, the time evolution of the ratio $\mathrm{DI^{13}C/DIC}$ matters rather than the evolution of individual concentrations. While the increases in individual $\mathrm{DI^{13}C}$ and

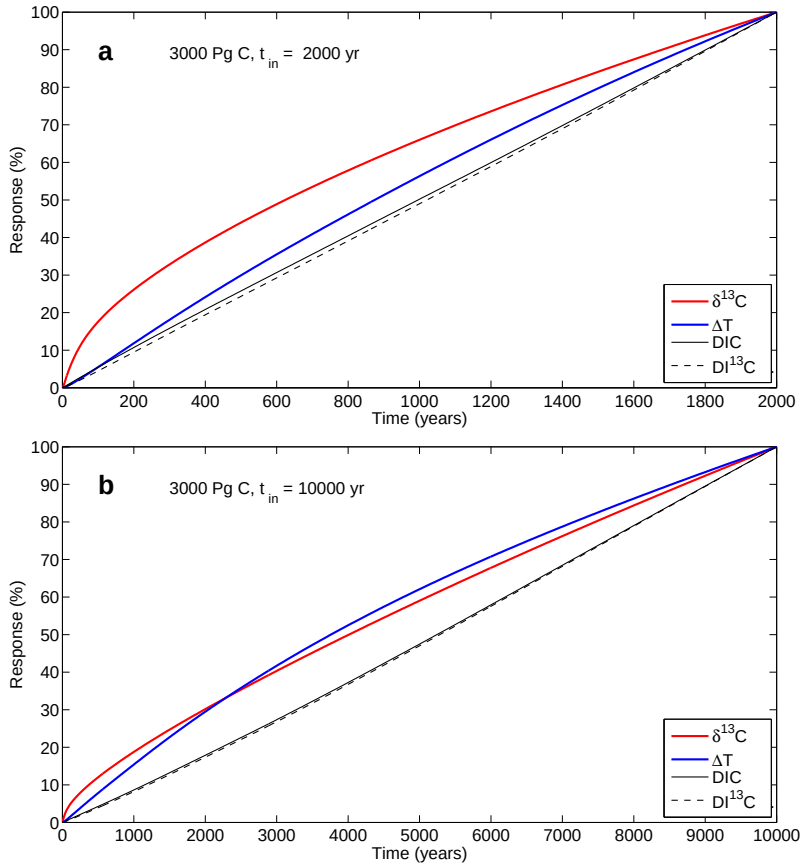

Figure S7. LOSCAR model results for carbon release times (t_{in}) of (a) 2,000 yr and (b) 10,000 yr (note different time axes). All model output is for the surface ocean and is normalized to 100% response at $t = t_{in}$ ($\delta^{13}\mathbf{C} = \delta^{13}\mathbf{C}_{\mathrm{DIC}}$; DIC = total dissolved inorganic carbon).

DIC are rather smooth, the normalized increase in DIC is slightly faster than in $DI^{13}C$ (Fig. S7) — the reason being that CO_2 equilibration is faster than carbon isotope equilibration[28]. As a result, the initial $DI^{13}C/DIC$ ratio and hence $\delta^{13}C_{DIC}$ drops rapidly (%response rises). In contrast, the initial temperature response over centuries is delayed due to the climate system's thermal inertia (see main manuscript). The normalized $\delta^{13}C$ response is thus faster than the normalized temperature response, provided the release time is a few millennia or less (Fig. S7a).

For much longer release times, the difference between CO_2 and carbon isotope equilibration becomes less important relative to the input time and the initial

drop in $\delta^{13}C_{DIC}$ (rise in normalized %response) is less pronounced (Fig. S7b). The temperature response, on the other hand, is hardly delayed on this time scale as the full surface warming is realized over many millennia. As a result, model temperature starts leading $\delta^{13}C$, which explains the sign reversal in τ_{mod} for long release times (see main manuscript).

In our model scenarios, the carbon mass is injected into the atmosphere, which is partly responsible for creating differences between surface CO_2 and carbon isotope equilibration and hence contributes to the rapid initial $\delta^{13}C_{DIC}$ surface response (Fig. S7). Alternatively, one could inject the carbon mass (or part of it) into the deep ocean, which would tend to reduce rapid changes in the surface $DI^{13}C/DIC$ ratio as result of atmospheric forcing. Hence we also tested a scenario in LOSCAR in which 3,000 Pg C were injected into the deep Atlantic instead of the atmosphere. The result was a substantial delay in the rise of atmospheric CO_2 (and hence temperature), which outweighed the less rapid initial surface $\delta^{13}C$ response (not shown). For millennial release times, the calculated model lag, τ_{mod}, was thus *longer* for deep-ocean carbon injection than for atmospheric injection. Because the goal here is to constrain the *minimum* onset time interval, the relevant scenario is hence atmospheric injection (yielding *shorter* model lags), rather than deep-ocean injection. All τ_{mod} discussed in the main manuscript were calculated for carbon injection into the atmosphere.

References

1. Wei, W. W. S. *Time Series Analysis: Inivariate and Multivariate Methods*. Addison-Wesley, pp. 478, (1990).

2. Chatfield, C. *The Analysis of Time Series: An Introduction*. CRC Press, pp. 333, 6th edition, (2004).

3. Box, G. E. P. & Jenkins, G. M. *Time Series Analysis: Forecasting and Control*. Holden-Day, San Franciso, CA, (1970).

4. Makarova, M., Miller, K. G., Wright, J. D., Rosenthal, Y., & Babila, T. Temperature and salinity changes associated with the Paleocene-Eocene Carbon Isotope Excursion along the mid Atlantic margin. *AGU Fall Meeting*, :Abstract PP33C–2322, (2015).

5. Zachos, J. C., Schouten, S., Bohaty, S., Sluijs, A., Brinkhuis, H., Gibbs, S., Bralower, T., & Quattlebaum, T. Extreme warming of mid-latitude coastal ocean during the Paleocene-Eocene Thermal Maximum: Inferences from TEX_{86} and isotope data. *Geology*, 34:737–740, (2006).

6. John, C. M., Bohaty, S. M., Zachos, J. C., Sluijs, A., Gibbs, S., Brinkhuis, H., & Bralower, T. J. North American continental margin records of the Paleocene-Eocene thermal maximum: Implications for global carbon and hydrological cycling. *Paleoceanogr.*, 23:PA2217, doi:10.1029/2007PA001465, (2008).

7. Arthur, M. A., Dean, W. E., Zachos, J. C., Kaminski, M., Hagerty Reig, S., & Elmstrom, K. Geochemical expression of early diagenesis in middle Eocene-lower Oligocene pelagic sediments in the southern Labrador Sea, Site 647, ODP Leg 105. In *Proc. ODP Sci. Results*, volume 105, pages 111–136, (1989).

8. Coleman, M. L., Hedrick, D. B., Lovley, D. R., White, D. C., & Pye, K. Reduction of Fe(III) in sediments by sulphate-reducing bacteria. *Nature*, 361:436–438, (1993).

9. Mozley, P. S. & Wersin, P. Isotopic composition of siderite as an indicator of depositional environment. *Geology*, 20:817, (1992).

10. Mozley, P. S. & Burns, S. J. Oxygen and Carbon Isotopic Composition of Marine Carbonate Concretions: An Overview: REPLY. *J. Sed. Petr.*, 63(5):1008, (1993).

11. Zachos, J. C., Bohaty, S. M., John, C. M., McCarren, H., Kelly, D. C., & Nielsen, T. The Paleocene-Eocene carbon isotope excursion: Constraints from individual shell planktonic foraminifer records. *Royal Society Phil. Trans. A*, 365:1829–1842, doi:10.1098/rsta.2007.2045, (2007).

12. Stassen, P., Thomas, E., & Speijer, R. P. Integrated stratigraphy of the Paleocene-Eocene thermal maximum in the New Jersey Coastal Plain: Toward understanding the effects of global warming in a shelf environment. *Paleoceanogr.*, 27:PA4210, (2012).

13. McInerney, F. A. & Wing, S. L. The Paleocene-Eocene Thermal Maximum: A Perturbation of Carbon Cycle, Climate, and Biosphere with Implications for the Future. *Ann. Rev. Earth Planet. Sci.*, 39(1):489–516, (2011).

14. Wright, J. D. & Schaller, M. F. Evidence for a rapid release of carbon at the Paleocene-Eocene thermal maximum. *Proc. Nat. Acad. Sci.*, 110:15,908–15,913, (2013).

15. Pearson, P. N. & Thomas, E. Drilling disturbance and constraints on the onset of the Paleocene-Eocene boundary carbon isotope excursion in New Jersey. *Clim. Past*, 11: 95–104, (2015).

16. Mann, M. E. & Lees, J. M. Robust estimation of background noise and signal detection in climatic time series. *Climatic Change*, 33(3):409–445, (1996).

17. Ridgwell, A. J. & Hargreaves, J. C. Regulation of atmospheric CO_2 by deep-sea sediments in an Earth system model. *Global Biogeochem. Cycles*, 21:doi:10.1029/2006GB002764, (2007).

18. Ridgwell, A. & Schmidt, D. Past constraints on the vulnerability of marine calcifiers to massive carbon dioxide release. *Nature Geosci.*, 3:196–200, doi:10.1038/ngeo755, (2010).

19. Archer, D., Eby, M., Brovkin, V., Ridgwell, A., Cao, L., Mikolajewicz, U., Caldeira, K., Matsumoto, K., Munhoven, G., Montenegro, A., & Tokos, K. Atmospheric lifetime of fossil fuel carbon dioxide. *Ann. Rev. Earth Planet. Sci.*, 37:117–134, (2009).

20. Zeebe, R. E., Zachos, J. C., & Dickens, G. R. Carbon dioxide forcing alone insufficient to explain Palaeocene-Eocene Thermal Maximum warming. *Nature Geosci.*, 2:576–580, doi:10.1038/ngeo578, (2009).

21. Zeebe, R. E. LOSCAR: Long-term Ocean-atmosphere-Sediment CArbon cycle Reservoir Model v2.0.4. *Geosci. Model Dev.*, 5:149–166, (2012).

22. Bice, K. L. & Marotzke, J. Could changing ocean circulation have destabilized methane hydrate at the Paleocene/Eocene boundary? *Paleoceanogr.*, 17:1018, doi:10.1029/2001PA00678, (2002).

23. Zeebe, R. E. Time-dependent climate sensitivity and the legacy of anthropogenic greenhouse gas emissions. *Proc. Nat. Acad. Sci.*, 110:13739–13744, (2013).

24. Dickens, G. R., O'Neil, J. R., Rea, D. K., & Owen, R. M. Dissociation of oceanic methane hydrate as a cause of the carbon isotope excursion at the end of the Paleocene. *Paleoceanogr.*, 10:965–971, (1995).

25. Sluijs, A., Brinkhuis, H., Schouten, S., Bohaty, S., John, C., Zachos, J. C., Reichart, G. J., Sinninghe Damste, J. S., Crouch, E. M., & Dickens, G. R. Environmental precursors to rapid light carbon injection at the Palaeocene/Eocene boundary. *Nature*, 450:1218–1221, (2007).

26. Hansen, J. and Russell, G. and Lacis, A. and Fung, I. and Rind, D. and Stone, P. Climate Response Times: Dependence on Climate Sensitivity and Ocean Mixing. *Science*, 229: 857–859, (1985).

27. Roe, G. Feedbacks, Timescales, and Seeing Red. *Ann. Rev. Earth Planet. Sci.*, 37:93–115, (2009).

28. Lynch-Stieglitz, J., Stocker, T. F., Broecker, W. S., & Fairbanks, R. G. The influence of air-sea exchange on the isotopic composition of oceanic carbon: Observations and modeling. *Global Biogeochem. Cycles*, 9:653–665, (1995).